How do the micropores of carbon xerogels influence their electrochemical behavior as anodes for lithium-ion batteries?

Marie-Laure C. Piedboeuf [1*], Alexandre F. Léonard [1,†], Gudrun Reichenauer [2], Christian Balzer [2] Nathalie Job [1]

[1] *Department of Chemical Engineering – Nanomaterials, Catalysis, Electrochemistry (NCE) University of Liège (B6a), 4000 Liège, Belgium*

[2] *Bavarian Center for Applied Energy Research, Division, Energy Efficiency, Magdalene-Schoch-Strasse 3, 97074 Wuerzburg, Germany*

Abstract

This work aims at shedding light on how the microporous texture of porous carbons influences their electrochemical behavior when used as anodes for Li-ion batteries. To this aim, a synthetic hard carbon (carbon xerogel, CX), prepared from a resorcinol-formaldehyde precursor gel, underwent several post-synthesis treatments in order to modulate its micropore to total pore volume ratio. The micropore volume was either expanded by physical activation or decreased using chemical vapor deposition (CVD) of a carbon layer.

Several variables other than the micropore texture of the obtained carbons, which could influence their behavior as anode active materials for Li-ion batteries, such as the particle size or the electrode characteristics, were carefully controlled. The thickness of electrode coatings and the pore texture of the active material-binder composite were analyzed. It was shown that CX-binder composites resulting from water-based slurries preserve the microporosity of the starting materials. Detailed electrochemical characterization of the electrodes prepared with carbon xerogels displaying various defined micropore textures was performed. A clear linear dependency could be evidenced between the Li^+ insertion and de-insertion in half-cell configuration with the increase of the volume of supermicropores (0.7 – 2 nm), demonstrating the effect of micropore enlargement by activation on the storage capacity, provided the maximum charge potential value is set at 3.0 V *vs.* Li^+/Li.

[*] Present address: AC&CS – CRM GROUP, Allée de l'Innovation 1, B - 4000 Liege (Belgium)

[†] Corresponding author. Tel: +32 4 366 3579. E-mail: alexandre.leonard@uliege.be (A.F. Leonard)

Keywords

Carbon xerogels, physical activation, Li-ion battery, microporosity, charge capacity, irreversible capacity

1. Introduction

Since the introduction of the Li-ion battery technology, carbon materials have extensively been studied and used as anode materials. The first Li-ion battery commercialized by Sony in 1991 included an anode prepared from a disordered carbon (coke) [1]. Nevertheless, the main drawback of this type of carbon lies in the fact that very high irreversible losses occur at the first charge-discharge cycle [2]. For that reason, it was replaced by graphite, which has remained until now the most appropriate carbon-based active material for this application, due to improved cycle life and fast rate capability compared to coke. However, the theoretical (and practical) capacity of graphite is limited to the insertion of one Li^+ per six carbon atoms (which corresponds to 372 $mAh.g^{-1}$), *i.e.* a much lower capacity than that observed for porous hard carbons for instance [3-4]. Moreover, the insertion mechanisms of Li^+ ions inside porous carbon structures still remains a matter of debate in the literature; in particular, the impact of the pore texture remains unclear.

In that respect, we recently published a first study concerning the use of carbon xerogels (CX) as model materials to better understand the behavior of porous carbons as anodes for Li-ion batteries [5]. Carbon xerogels are usually made of a hierarchical pore texture featuring microporous nodules that delimitate meso- or macroporous voids [6]. Standardized synthesis conditions based on resorcinol-formaldehyde as precursor lead to materials with micropore volumes between 0.15 and 0.30 $cm^3.g^{-1}$. The meso- or macropore size can be controlled by the synthesis conditions (pH mainly) and can be varied over a wide range, from 5 nm to 5000 nm. In the above-mentioned study [5], where polyvinylidene fluoride (PVDF) was used as a binder, it was concluded that the external surface area of the CX backbone, representing the surface of

meso- or macropores, is a more appropriate parameter than its total specific surface area to explain the observed electrochemical behavior: indeed, the insertion/de-insertion capacity was directly linked to the external surface of the carbon nodules, while the micropores were blocked by the PVDF binder. Going a step further, another work shed some light on the importance of the binder used for the electrode preparation when porous materials are involved [7]. Indeed, the processing of active materials into electrodes can strongly affect the textural characteristics of the final composite formed by the porous active material and the binder.

Post-synthesis treatments can be applied to carbon xerogels to selectively modulate the micropore volume without altering the meso- or macropore structure. The micropore volume can be increased by chemical (using *e.g.* KOH or $ZnCl_2$) or physical (using *e.g.* steam or CO_2 at elevated temperature) activation. In particular, for carbon xerogels, CO_2 physical activation was compared with chemical activation using hydroxides [8]. It was concluded that physical activation has numerous advantages such as the possible coupling with the pyrolysis step, the retention of the meso- or macropore texture and the preservation of the surface chemistry. On the opposite, a decrease of the microporosity can be achieved, for instance, by chemical vapor deposition (CVD) of carbon initiated by ethylene cracking. Since CVD is an efficient technique for the nano-replication of zeolites or mesoporous silica into porous carbons, it can be assumed that the precise control of the conditions could lead to a selective filling or blocking of the microporosity of the CX without affecting significantly the large pores [9].

In the literature, activated porous carbons derived from organic gels have been evaluated as anode materials for Li-ion batteries [10–12], among which highly microporous carbon aerogels and xerogels activated by chemical [10] or physical [11–12] post-treatments. In all cases, the reversible charge capacity was enhanced (from 200 $mAh.g^{-1}$ for the pristine carbon up to 700 $mAh.g^{-1}$), and the irreversible capacity at the first cycle increased as well (from 300 to 3000 $mAh.g^{-1}$). The main issue is that, even though both capacities globally increase with activation, no correlation was found between the specific surface area measured on the powder and the

irreversible and reversible capacities. Even for similar values of specific surface area, differences in the absolute values of stored energy can be noticed in some cases. In addition, no information is provided regarding either the meso- and macropore texture of the carbons, or the final pore texture in the electrode composite, prepared using PVDF as a binder. Since PVDF is known to block micropores [5, 7], it is no surprise that the electrochemical data seem scattered. Also, the particle size is never reported, while it can affect Li^+ (de)insertion. Finally, the maximum potential value used for electrochemical characterization changes from one study to another (2.0 to 3.0 V *vs.* Li^+/Li), which could also lead to different conclusions. It is therefore difficult to derive general trends. In particular, a more systematic study using a binder that leaves the micropore surface accessible to the electrolyte is necessary to compare results and establish relationships between the microporosity and/or the specific surface area of the material, and its behavior as Li-ion electrode material.

The aim of the present study is thus to isolate the sole influence of the micropores of porous carbons on their electrochemical behavior as anodes for Li-ion batteries while keeping constant all other variables such as the meso- and macropore texture, the particle size and the electrode processing method. For that purpose, a macroporous carbon xerogel (with an average pore size of 80 nm) was selected and submitted to different treatments in order to selectively modulate its micropore fraction. The samples were carefully analyzed in terms of pore texture characteristics but also in terms of preservation of the particle size. Moreover, an original process was used for the preparation of the electrodes, which allows the retention of the initial porous properties of the powder when processed as the final electrode. Finally, the electrochemical behavior as anodes for Li-ion batteries was evaluated, and a relationship with the textural parameters of the samples was established.

2. Experimental

2.1. Synthesis of the pristine carbon xerogel

The material studied was prepared following the process described by Job *et al.* [6]. In brief, a 35 wt.% resorcinol (Merck) aqueous solution was prepared and the pH was set by addition of powdery sodium carbonate. A 37 wt.% solution of formaldehyde stabilized by 10-15 wt.% methanol (Sigma-Aldrich) was then added in a molar ratio resorcinol : formaldehyde equal to 1 : 2 and the mixture was magnetically stirred for 1 h. The molar dilution ratio D = water/reactants was fixed at 5.7. The molar ratio between resorcinol and carbonate (R/C) was chosen equal to 2000. The obtained homogeneous gel precursor solution was then sealed in a 250 mL autoclaveable glass flask and aged for 3 days at 85°C. After gelation and ageing, drying was performed by placing the gel in an oven under vacuum (2 kPa) at 60 °C for 12 h and then at 150 °C for 30 h.

The dry xerogel was then ground using a Fritsch planetary mill (Mono Mill P6) in agate jars with 1 cm diameter agate balls following the procedure described in a previous work to obtain homogenous and reproducible particle sizes [13]. The obtained powder was put in a quartz boat and introduced in a ceramic tubular oven to undergo a pyrolysis step at 900 °C, leading to a carbon xerogel. The pyrolysis was performed just before coating on current collectors or other post-synthesis treatments, under nitrogen (Air Liquide Alphagaz 1, flow rate = 0.004 mol.min^{-1}) with the following temperature profile: (1) ramp at 1.7 °C/min to 150 °C and hold for 15 min; (2) ramp at 5 °C/min to 400 °C and hold for 60 min; (3) ramp at 5 °C/min to 900°C and hold for 120 min; and (4) natural cooling to room temperature. This (reference) carbon xerogel pyrolyzed at 900°C without any other treatment is hereafter denoted CX-Ref.

2.2. Physical activation with CO_2

The physical activations were performed using CO_2 in the same tubular oven as used for the pyrolysis. The oven was connected to a nitrogen and a carbon dioxide supply *via* a three-way valve, allowing to switch between both atmospheres. 5 g of the powdery dry polymer gel were

introduced in the tubular oven to undergo a pyrolysis at 900 °C for 2 h under nitrogen as described above; subsequently, the atmosphere in the tube was modified by switching from the nitrogen supply to the CO_2 bottle (Air Liquide N27), still at 900 °C and by keeping the same flow rate of 0.004 mol.min^{-1}. This temperature was maintained for different durations necessary for the activation process (3, 8 or 16 h). Finally, the cooling step was done under nitrogen atmosphere. The different samples are denoted as follows: CX-A is followed by the activation time in hours. For instance, CX-A3 denotes a carbon xerogel that underwent a physical activation for 3 h.

2.3. Chemical vapor deposition of ethylene

Chemical vapor deposition was performed in a stainless steel tubular oven. The temperature of the oven was set at 685 °C under inert atmosphere (flow rate: 0.025 mol.min^{-1}). The untreated CX sample was placed in a quartz boat and introduced in the oven at this temperature by using a reverse flow system allowing to keep the protective inert atmosphere. The reactor was then fed with a gaseous mix (total flow rate: 0.082 mol.min^{-1}) constituted of 80 % of ethylene (Air Liquide N25, 0.066 mol.min^{-1}) and 20 % of nitrogen (Air Liquide Alphagaz 1, 0.016 mol.min^{-1}) for 30 min at 685 °C. Then, the atmosphere was modified to 100 % of nitrogen (flow rate: 0.025 mol.min^{-1}). Finally, the temperature was increased to 900 °C and kept constant for another 2 h. This step was followed by cooling under nitrogen atmosphere. The resulting sample is denoted CX-CVD.

2.4. Preparation and characterization of electrodes

After grinding and pyrolysis, the materials were processed into electrodes. The final powders were kept in a glove box under argon atmosphere (MBraun) before coating to avoid a possible modification of the surface chemistry upon exposure to air. A powdery mix containing CX and xanthan gum (XG, Sigma-Aldrich, binder) was suspended in ultra-pure water to form a homogeneous slurry. In a typical slurry preparation, the CX and XG mass fractions were set at 88 – 12 wt. % respectively in the solid mix, and the amount of water added was chosen so that

the solid (CX + binder) to water mass ratio was 50 wt. %. This ink was then sprayed manually (Harder & Steenbeck Evolution Silverline 2) on pre-weighed stainless steel disks (Ø: 15.5 mm, MTI corporation, stainless steel 304, thickness: 0.5 mm), homogeneously dispersed on a protecting aluminum foil. The formed coatings were left to dry for 1 h at ambient temperature, followed by 16 h at 60 °C and finally 3 h under vacuum at 120 °C. The formed electrodes were then directly introduced into an Ar-filled glovebox (MBraun). The excess of dry ink sprayed next to the electrodes on the protecting aluminum foil was scratched-off from the support and recovered, allowing for obtaining a powdery active material-binder composite that displays the same textural parameters as those of the electrodes.

The thickness of the coatings after drying was measured by stylus profilometry (Veeco Dektak 150, stylus radius: 12.5 µm, force: 9.8 µN). In order to get access to the thickness of the coatings, three electrodes were fixed on a glass slide as illustrated in Fig.S.I.1. The carbon layer was scratched off from borders to get access to the baseline. The thickness was calculated as an average value taken from the two pathways on each electrode with two scans each.

2.5. Pore texture and particle size characterization

The pore texture of both the powdery carbon xerogels and the corresponding carbon-binder composites forming the electrodes, was characterized by nitrogen adsorption. The nitrogen adsorption-desorption isotherms were measured at -196 °C using a volumetric analyzer (ASAP 2420, Micromeritics, Norcross, USA). The samples were degassed overnight, at 270 °C for the starting carbon or 120 °C for the carbon-binder composites, under high vacuum (133 Pa) prior to analysis. From the nitrogen adsorption isotherms, the specific surface area, S_{BET}, was calculated using the Brunauer-Emmett-Teller (BET) equation, with the adsorption data selected in the relative pressure range 0.01 to 0.10 [14]. The specific external surface area of the nodules, S_W, *i.e.* here the surface corresponding to the macropores, was determined following the method described by Magee [15].

To access the evolution of microporosity of the powders in the complete pore size range between about 0.3 and 2.0 nm, in addition to N_2 adsorption at -196 °C, CO_2 adsorption analysis at 0 °C was performed using a volumetric adsorption instrument (ASAP 2020, Micromeritics, Norcross, USA). Prior to analysis, the samples were degassed at 300 °C and under vacuum (133 Pa) for about 24 h. It should be mentioned that these measurements were carried out only on the starting pure carbon materials.

To determine the specific micropore volume and surface area distributions of the carbons, we performed a combined nonlocal density functional (NLDFT) analysis of N_2 and CO_2 adsorption isotherms using models for slit-shaped carbon pores based on refs [16-20]. Data analysis was carried out using the commercial software Microactive (Micromeritics, Norcross, USA) [21]. From these datasets, the average micropore width w was calculated as:

$$w = 2S_{\mathrm{mic,NLDFT}}/V_{\mathrm{mic,NLDFT}} \quad [1]$$

with $S_{\mathrm{mic,NLDFT}}$ and $V_{\mathrm{mic,NLDFT}}$ being the integral of the specific micropore surface area and volume, respectively, as derived from the respective distributions.

Since the carbon xerogel samples feature macropores, the nitrogen adsorption technique is not suitable for the determination of the respective pore width and pore volume. For that reason, mercury porosimetry was performed with a Quantachrome Poremaster 60 in a pressure range comprised between 0.01 to 400 MPa. The analysis of the obtained mercury intrusion data allows for determining the specific pore volume, V_{Hg}, as well as the pore size distribution for pores larger than 3.8 nm in diameter. The latter was calculated by using the Washburn equation [22], valid for mercury intrusion without crushing and upon using average values of the liquid/solid contact angle of 140° and a surface tension of mercury of 0.485 $N.m^{-1}$.

Furthermore, the particle size distribution of the powders was obtained using laser diffraction with a Mastersizer 2000 (Malvern Instruments) in wet mode (Hydro2000). Prior to grain size distribution measurements, the samples were dispersed in water using high intensity ultrasonic irradiations (Hielsher, UP400S). The sample preparation method is fully described elsewhere

[13]. Particle size distributions were obtained from the raw data by mathematic treatment assuming a spherical geometry of the particles.

2.6. Electrochemical characterization

The electrochemical measurements were carried out in CR2032 coin cells, where the tested material acted as positive electrode and a Li-metal disk as the negative, reference and counter electrode. A Celgard® separator soaked with 80 µL of LP71 (1 M $LiPF_6$ in EC:DEC:DMC 1:1:1) electrolyte was placed in-between. The cell assembly was performed in an Ar-filled glove-box (MBraun). Charge-discharge cycles were recorded at C/10 (*i.e.* using the necessary current to charge completely the battery in 10 h, based on the theoretical value for graphite – 372 $mAh.g^{-1}$) between 0.005 and 1.5 V or 3.0 V *vs.* Li^+/Li with a potentiostat (Biologic VMP3 multichannel) or a battery tester (Neware BTS 5 V / 1mA) at a controlled temperature of 25 °C. Cyclic voltammetry was also performed in the same voltage range at a scan rate of 0.05 $mV.s^{-1}$.

In order to evaluate the surface accessibility by the electrolyte, capacitance measurements in capacitor configuration were performed by using CX electrodes at each pole of the coin cell as described elsewhere [5]. The electrolyte used was the same as for the half-cell assembly and the cell voltage ranged from -0.3 to 0.3 V. Cyclic voltammetry was performed at a speed of 20 $mV.s^{-1}$ and the capacitance was calculated from the slope of the straight line obtained by plotting the charge (q) versus the potential (V). Graphite (KS6L, Timcal) was used in order to compare the electrochemical behavior of CX material with a commercial carbon material used as anode for Li-ion battery.

3. Results and discussion

3.1. Pore texture of the carbon xerogels

The nitrogen and carbon dioxide isotherms of all carbon xerogels investigated in this work are shown in Figures 1a and 1b, respectively, while the analysis results according to BET theory,

t-plot method and NLDFT are given in Table 1. As can be seen from Figure 1, the nitrogen adsorption isotherms of all samples investigated are combined type I and II isotherms according the IUPAC recommendations [14]; as such, all samples feature micro- and macroporosity.

To begin with, we consider the reference carbon xerogels CX-Ref and the species activated for 3, 8 and 16 h, *i.e.* the samples CX-3, CX-8 and CX-16. As expected, all data evaluation techniques show an increase in specific micropore volume and respective surface area for progressing activation. Fig. S.I.2 shows a plot of the mass loss of the dry polymer gel powders after pyrolysis and activation as a function of the activation time. For the pyrolyzed powder without any other treatment (activation time = 0 h), a 52 % mass loss is observed, which is in line with previous results [6]; it corresponds to the carbonization of the polymer network, *i.e.* the end of the pyrolysis step. The CO_2 activation induces an additional and increasing mass loss linked to the activation time, up to 36 % after 16 h of treatment. This results from the progressive erosion of the carbon by the carbon dioxide following the Boudouard reaction [23]. In contrast to the activated samples, the carbon xerogel subjected to CVD treatment displays a mass increase of 25 %, confirming the deposition of a carbon coating.

Table 1: Textural parameters associated to nitrogen adsorption isotherms presented in Fig. 1.

Sample	S_{BET} ($m^2.g^{-1}$) [a]	S_W ($m^2.g^{-1}$) [b]	$S_{mic,NLDFT}$ ($m^2.g^{-1}$) [c]	V_{NLDFT} ($cm^3.g^{-1}$) [c]
	± 5 %			
CX-CVD	112	98	99	0.025
CX-Ref	679	124	908	0.247
CX-A3	1162	168	1397	0.426
CX-A8	1723	244	1684	0.618
CX-A16	2234	507	1788	0.788

[a] Calculated by the BET equation in the P/P_0 range 0.01-0.10 [14].

[b] Calculated by the method described by Magee [15].

[c] Calculated by NLDFT analysis of combined nitrogen and carbon dioxide isotherms.

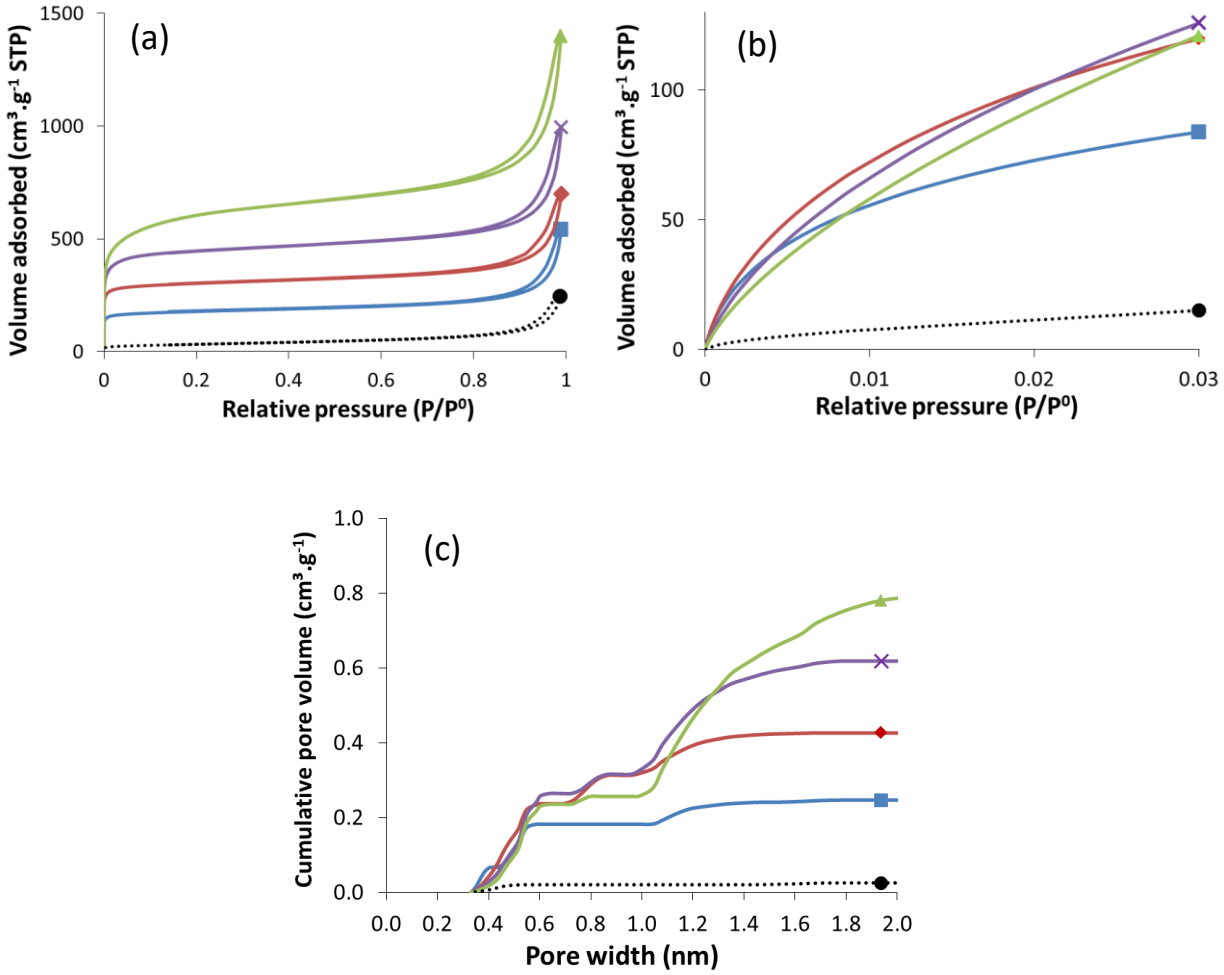

Figure 1: (a) N_2 adsorption-desorption isotherms; (b) CO_2 adsorption isotherms; (c) Micropore volume as a function of pore width. (■) CX-Ref, (◆) CX-A3, (×) CX-A8, (▲) CX-A16 and (●) CX-CVD.

The values of specific BET surface area as derived from N_2 isotherms are reported in Table 1 for comparative purposes with other studies, since this theory is the most widely applied in textural analysis. Nevertheless, the calculations are not the most appropriate for micro-mesoporous carbon xerogels, which is the reason why, in the present case and in order to be more accurate regarding the micropore fraction of the materials, we chose to focus the discussion on the data calculated from the nonlocal density functional (NLDFT) analysis of combined N_2 and CO_2 adsorption isotherms. The micropore area of the unmodified carbon

xerogel CX-ref equals 908 $m^2.g^{-1}$. In the case of CX-CVD, this value is sharply reduced down to 99 $m^2.g^{-1}$. On the opposite, the specific surface area increases with the activation time, with values up to 1788 $m^2.g^{-1}$ for CX-A16. The cumulative micropore volume for pores with sizes comprised between 0.3 and 2.0 nm follows the same trend (see Figure 1c). In addition to the substantial increase in microporosity following the activation process, which was the main aim here, the data also point to a development of the external surface area S_W of the nodules (Table 1). This could be related to a decrease in the size of the nodules, to the evolution of mesoporosity on the outer surface of the latter, or a combination of both, upon activation.

Mercury intrusion porosimetry allows obtaining the total specific volume of pores larger than 3.8 nm. Since the present study is focused on the microporosity effect, the Hg porosimetry results are presented in Supplementary Information (see Figure S.I.3). Globally, the macropore texture is retained, both after CVD treatment or activation, even though the average pore size tends to decrease when the activation time is long (8 or 16 h). This phenomenon is likely due to a broadening of the pore size distribution and not to the shrinking of the pores already present in the material. This observation could explain the increase in the external surface area if the nodules are subjected to mesopore formation on their surface, especially after the harsh activation treatments.

3.2. Powder and coating characterization

Laser granulometry analysis of the powders (Figure S.I.4) shows that the final particle size distribution of the powders is not significantly affected by the physical activation treatment. Particle size distributions coincide for all samples except the one treated by CVD: in the case of the latter, the particle size distribution is shifted to slightly higher values, which could be explained either by the fact that the additional carbon coats both the micropores and the external surface of the particles or (more likely as the particle size distribution is shifted by several µm) by an agglomeration of different particles together, inducing increased particle sizes.

The thickness of the electrode coatings (Table S.I.2), measured by stylus profilometry technique, is similar for CX-Ref and CX-CVD; it however increases when the samples are activated. Indeed, the activation process strongly decreases the bulk density of the carbon, leading to a thicker coating for a similar mass of active material (214 µm for CX-A16 compared to 96 µm for CX-Ref).

The textural properties of the final composites formed between the CX active material and the binder were evaluated by N_2 adsorption-desorption. As described in the experimental part, this composite is recovered from the excess of dry ink and thus really reflects the pore texture of the electrodes. Fig. 2 compares the N_2 adsorption-desorption isotherms of the bare powders with the corresponding composites.

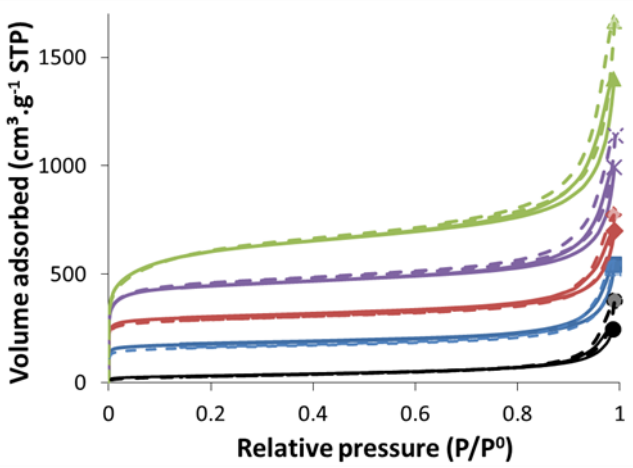

Figure 2: Comparison of N_2 adsorption-desorption isotherms: (■) CX-Ref, (◆) CX-A3, (×) CX-A8, (▲) CX-A16 and (●) CX-CVD. The continuous line represents the bare powder and the dotted line represents the corresponding composite.

The data corresponding to the composites were corrected so as to take only the carbon into account, since the binder is considered as a non-porous component. As seen from Fig. 2, the isotherms obtained for the powders and the corresponding composites are almost identical in the low to medium relative pressure regime (reflecting micropore and surface area characteristics), indicating that the pore texture of the composite processed as an electrode is the same as that of the pristine active material, especially regarding the specific micropore

volume and surface area.

Generally, when PVDF is used as binder for the preparation of electrodes made of porous carbons, the specific micropore volume of the resulting active material-composite is strongly reduced. In this context, this result is important since the method selected for this study allows preserving the initial microporous texture of powders. This conclusion is in line with a previous work [7] where PVDF, solubilized in N-methyl pyrrolidone (NMP), was replaced by a combination of Na-CMC and SBR in a water-based ink. Indeed, it was shown that the solvent used for ink preparation (NMP or water) has a strong influence on the final texture of the composite. It has been hypothesized that NMP enters the inner part of the material while water does not, leading in the latter case to almost no loss of porosity compared to the pristine powder [7].

3.3. Electrochemical characterization

The surface of the material (as composite in an electrode, with XG as binder) accessible to the electrolyte was analyzed in supercapacitor configuration as described in detail in our previous study [5], with the same electrolyte as that used for the electrochemical characterization in half-cells. Fig. 3a presents the cyclic voltammetry curves obtained at a scan rate of 20 $mV.s^{-1}$ for the different samples and Fig. 3b shows the calculated specific capacitance values for each sample. Clearly, the specific capacitance evolves with the treatment of the carbon component as expected.

The specific capacitance is clearly linked to the surface of the electrode accessible by the electrolyte. A significant increase in capacitance is observed when an activation treatment is applied. Indeed, the specific capacitance increases sharply after 3 h of physical activation (more than 25 $F.g^{-1}$ compared to 5 $F.g^{-1}$ for CX-Ref). A longer activation time increases the capacitance but the values seem to level off after 8 h treatment.

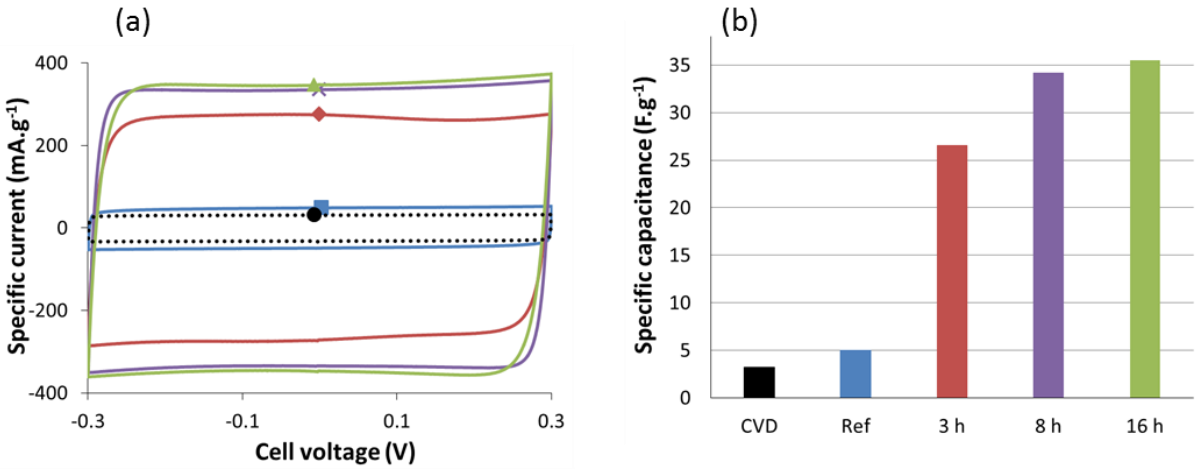

Figure 3: (a) Cyclic voltammetry curves obtained at a scan rate of 20 $mV.s^{-1}$ with the supercapacitor type assembly for (■) CX-Ref, (◆) CX-A3, (×) CX-A8, (▲) CX-A16 and (●) CX-CVD and (b) associated values of calculated specific capacitance

This phenomenon could be explained by a kinetic effect since the measurements are realized using high scan rates (20 $mV.s^{-1}$), much higher than those generally used in CV analysis performed on electrodes for Li-ion batteries. In contrast, the CVD treatment, reducing the micropore volume accessible to N_2 and CO_2 molecules, results in a 30% decrease in specific capacitance (3.2 $F.g^{-1}$ compared to 5.0 $F.g^{-1}$ for CX-Ref). Obviously, the capacitance in electrodes prepared from CX-CVD and CX-Ref samples are dominated by the external surface area, *i.e.* storage sites in micropores are not accessible to the ions because of either kinetic or steric limitations. With activation, access of ions to micropores is provided and the capacitance strongly increases. However, no direct correlation can be evidenced with the further increase in the micropore surface area with activation duration, so that the capacitance rather tends towards a maximum value. This described tendency is further illustrated in Fig. 4 showing the calculated specific capacitance as a function of the micropore surface area. The value of capacitance levels off, showing that the further increase in microporous surface does not result in a linear increase in accessible storage sites.

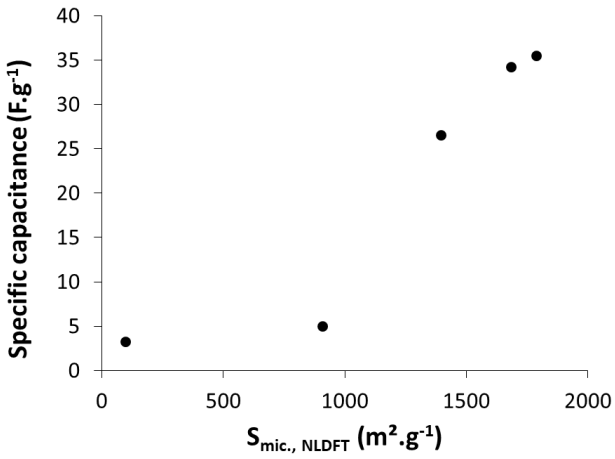

Figure 4: Specific capacitance as a function of the micropore surface area ($S_{mic.,NLDFT}$).

Fig. 5a presents experimental data derived for a half-cell lithium ion battery assembly in the first galvanostatic charge and discharge cycle obtained for the five samples at a rate of C/10 (*i.e.* using the necessary current to charge completely the battery in 10 h, based on the theoretical value for graphite – 372 mAh.g^{-1}). Fig. 5b shows the evolution of the charge capacity for the assemblies with the different carbon components (CX) upon cycling. Table 2 summarizes the numerical values associated to these measurements.

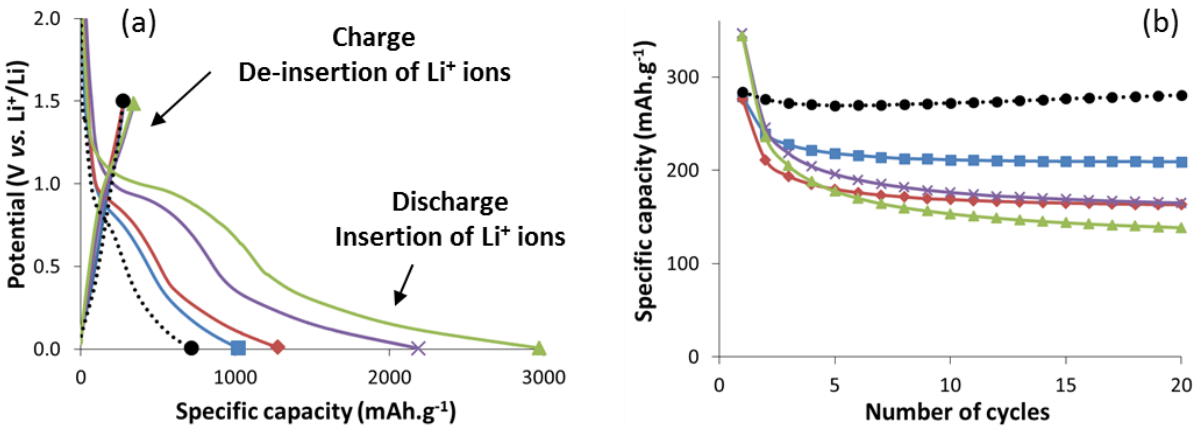

Figure 5: (a) Galvanostatic charge-discharge curves at the first cycle at a rate of C/10. (b) Reversible specific capacities at a rate of C/10 during 20 cycles. (■) CX-Ref, (◆) CX-A3, (×) CX-A8, (▲) CX-A16 and (●) CX-CVD.

Considering the first discharge, corresponding to the insertion of Li^+ ions inside the CX structure and to the formation of the solid electrolyte interface (SEI), it can be seen from the comparison of the curves in Fig. 5a that the specific capacity strongly increases with the duration of physical activation, and thus with the total accessible specific surface area *i.e.* the sum of $S_{mic,NLDFT}$ and S_W. On the other hand, the CVD treatment leads to a decrease of this value compared to the reference material. Concerning the charge step, which corresponds to the de-insertion of Li^+ ions from the carbon structure, a slight increase in capacity is observed with texture modification, but its extent is much more limited. Moreover, as shown in Fig. 5b, even if the charge capacity for the activated samples is higher at the first cycle, it decreases rapidly with further cycling and the values obtained after 20 cycles are in each case lower than that corresponding to CX-Ref. On the opposite, CX-CVD keeps a stable and higher reversible charge capacity compared to the reference material.

Table 2: Numerical values associated with electrochemical measurements performed at a maximum potential value of 1.5 V *vs.* Li^+/Li.

Sample	1st cycle			20th cycle
	Q_{irr}[a] (mAh.g^{-1})	Q_{rev}[b] (mAh.g^{-1})	Q_{irr}/Q_{rev}[c] (-)	Q_{rev}[b] (mAh.g^{-1})
	± 5 %	± 5 %	± 0.1	± 5 %
CX-CVD	452	276	1.6	268
CX-Ref	751	281	2.7	212
CX-A3	1015	269	3.9	165
CX-A8	1813	343	5.3	162
CX-A16	2589	334	7.8	135

[a] Irreversible capacity at the first cycle of charge-discharge: $Q_{irr} = Q_{disch1}-Q_{ch1}$ (Q_{disch1} corresponds to the capacity at the first discharge and Q_{ch1} corresponds to the capacity at the first charge).
[b] Reversible capacity corresponding to the charge capacity of the half-cell (Q_{ch}).
[c] Ratio between the irreversible capacity and the reversible capacity at the first charge-discharge cycle.

The Q_{irr}/Q_{rev} ratio (Table 2), calculated from the first charge-discharge cycle, is a parameter that can be used in order to get a better insight into the global behavior of the material as anode for a Li-ion battery. Indeed, this parameter takes into account both the irreversible losses and the reversible capacity contribution. For an ideal active material of Li-ion battery, this ratio

should tend to zero. Moreover, it is independent of the mass of active material, thereby precluding any possible error due to weighing of the electrodes [5]. The calculated ratio decreases for CX-CVD compared to the reference material, indicating a better electrochemical behavior. On the opposite, the ratio increases sharply with the activation time, due to a strong increase of the irreversible losses. Indeed, the absolute value of Q_{irr} is very high in the case of CX-A16 (2589 mAh.g^{-1}), which probably corresponds to a huge formation of the SEI on the accessible surface in combination with a massive insertion of Li^+ ions inside the micropores of the carbon structure.

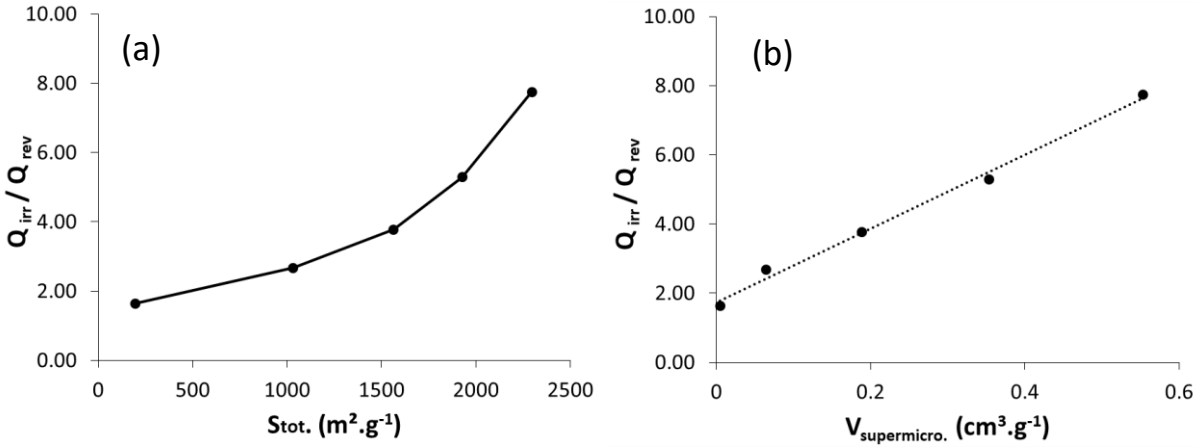

Figure 6: Q_{irr}/Q_{rev} at the first cycle as a function of (a) total accessible surface area (S_{tot} = $S_{mic,NLDFT}$ + S_w) and (b) the calculated cumulative volume of supermicropores (0.7–2.0 nm), as calculated from Fig. 1c.

The change of Q_{irr}/Q_{rev} with the total accessible surface area and the volume of micropores in the range between 0.7 and 2.0 nm (supermicropores) is further illustrated in Fig. 6. The data corresponding specifically to the micropores as obtained from the combination of N_2 and CO_2 adsorption measurements were further refined upon plotting the cumulative micropore volume as a function of the micropore sizes (Fig. 1c). The activation process makes additional ultramicropores (< 0.7 nm) accessible, but their pore volume does not further evolve with activation duration. On the opposite, a strong increase in both supermicropores (0.7-2.0 nm)

size and volume takes place with extending the activation time. Interestingly, as shown from Fig. 6b, a linear relationship can clearly be established between the supermicropore volume and the Q_{irr}/Q_{rev} ratio, suggesting that the massive insertion of Li ions at the first cycle is mostly controlled by the larger micropores. The offset in Fig. 6b indicates the contribution of the external surface area to the irreversible capacity.

In the previous experiments, the maximum charge potential value for the electrochemical characterization in the half-cells was voluntarily fixed at 1.5 V *vs.* Li^+/Li, with the aim of keeping conditions as close as possible to the working conditions of an anode material in a real Li-ion battery. Nevertheless, studies on activated materials in the literature are generally performed in a wider potential window (up to 2.0 or 3.0 V *vs.* Li^+/Li) [10–12]. To allow for a comparison with these values and to reach a better understanding of the phenomena occurring in porous carbon materials when used as anodes for Li-ion batteries, the same electrochemical characterizations were performed by setting the maximum charge potential at 3.0 V *vs.* Li^+/Li. Fig. 7a presents the curves corresponding to the first cycle of charge-discharge obtained for the five samples at a rate of C/10. Fig. 7b shows the evolution of the reversible capacity of CX samples upon cycling. Table 3 summarizes the numerical values associated to those measurements.

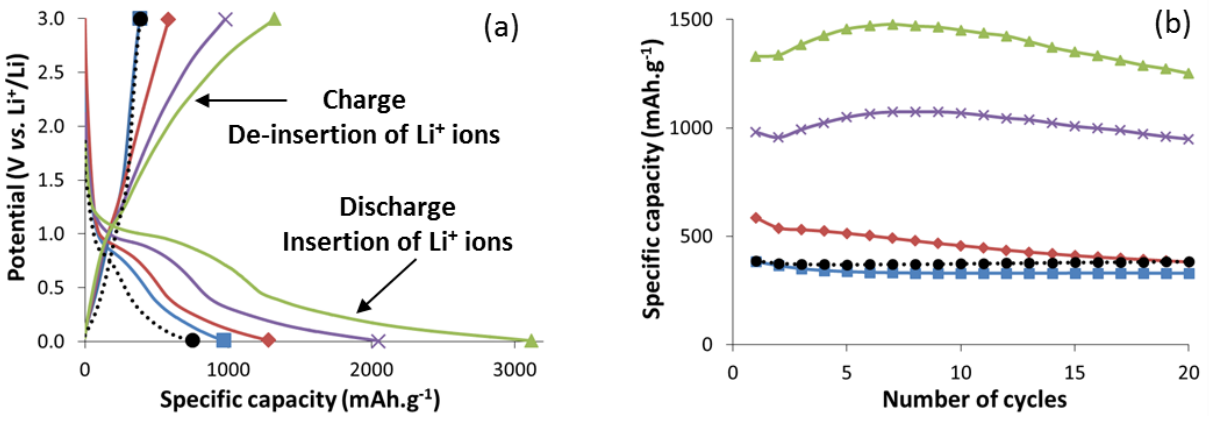

Figure 7: (a) Galvanostatic charge-discharge curves at the first cycle at rate of C/10. (b) Reversible specific capacities at rate of C/10 during 20 cycles. (■) CX-Ref, (◆) CX-A3, (×) CX-A8, (▲) CX-A16 and (●) CX-CVD.

From Fig. 7a, it can be seen that, for all activated CX, a significant additional charge capacity is present beyond 1.5 V and up to 3.0 V *vs.* Li^+/Li. The longer the activation duration, the lower the slope of the curve above 1.5 V *vs.* Li^+/Li. Considering the absolute values, the reversible capacity at the first charge cycle reaches 1330 $mAh.g^{-1}$ for CX-A16. Increased values of charge capacity are further maintained upon cycling up to 20 cycles (Fig. 7b), which was not the case when the potential was limited to 1.5 V *vs.* Li^+/Li.

The discharge capacity at the first cycle (first insertion of Li^+ ions) is independent of the used potential window. Nevertheless, since the reversible capacity is increased for activated samples with the larger voltage window, the relative irreversible losses are significantly reduced. Indeed, the value of Q_{irr} is calculated by subtracting the charge capacity from the discharge capacity at the first cycle. As the deinsertion (charge) capacity becomes much more important, the irreversible losses are strongly decreased. As a consequence, in this case the Q_{irr}/Q_{rev} ratio does not increase as for the characterization with the potential window limited at 1.5 V *vs.* Li^+/Li, but rather remains almost constant for all the studied samples.

Table 3: Numerical values associated with electrochemical measurements performed at a maximum potential value of 3.0 V *vs.* Li^+/Li.

Sample	**1st cycle**			**20th cycle**
	Q_{irr}[a] **(mAh.g^{-1})**	Q_{rev}[b] **(mAh.g^{-1})**	Q_{irr}/Q_{rev}[c] **(-)**	Q_{rev}[b] **(mAh.g^{-1})**
	± 5 %	± 5 %	± 0.1	± 5 %
CX-CVD	379	386	1.0	383
CX-Ref	593	383	1.5	329
CX-A3	710	585	1.2	381
CX-A8	1066	981	1.1	949
CX-A16	1794	1330	1.3	1251

[a] Irreversible capacity at the first cycle of charge-discharge: $Q_{irr} = Q_{disch1}-Q_{ch1}$ (Q_{disch1} corresponds to the capacity at the first discharge and Q_{ch1} corresponds to the capacity at the first charge).
[b] Reversible capacity corresponding to the charge capacity of the half-cell.
[c] Ratio between the irreversible capacity and the reversible capacity at the first charge-discharge cycle.

These results clearly show that the contribution of micropores is even more significant when the characterization is performed up to high potential values (3.0 V *vs.* Li^+/Li): indeed, during

the first discharge, Li^+ ions are massively inserted inside the CX samples (up to 3000 $mAh.g^{-1}$ for CX-A16). Li^+ ions are only partially extracted when the charge step (Li^+ de-insertion) is performed up to 1.5 V *vs.* Li^+/Li. Raising this potential value up to 3.0 V *vs.* Li^+/Li allows for a much more significant de-insertion of the Li^+ from the structure of the activated carbon xerogels. Concerning the CX-CVD sample, the potential value increase does not change the tendency observed in comparison with the reference material. Indeed, in this sample, the volume corresponding to micropores is strongly reduced. This further confirms the predominant contribution of supermicropores (0.7 to 2 nm) to the massive insertion and deinsertion of Li ions when cycling is performed up to a higher potential.

3.4. Comparison with graphite

In order to shed some light on the differences between the behavior of graphite (generally used as anode in a Li-ion battery) and porous carbons, electrodes of graphite were prepared under the same conditions as for the CX samples (same current collector, same binder, no conductive additive and no pressing of the coating). Fig. 8 compares the electrochemical behavior of an electrode made of CX-A16 with the one made with graphite.

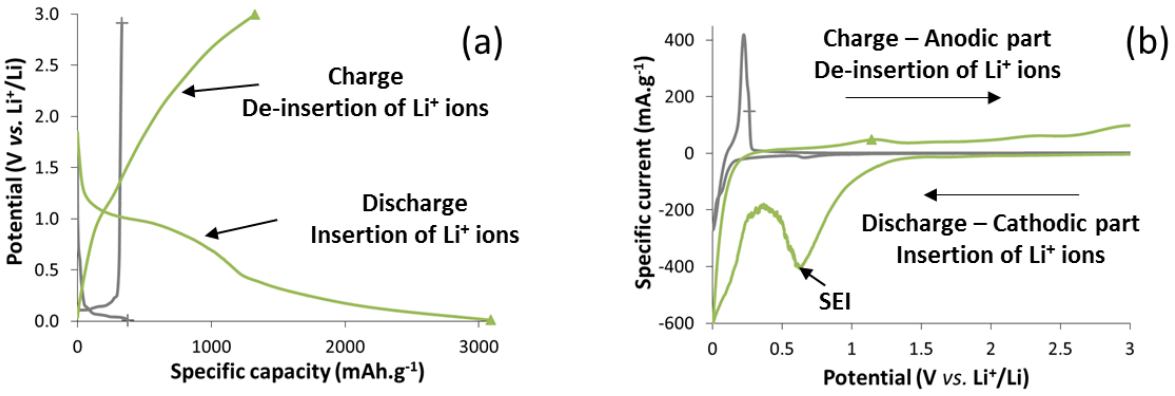

Fig. 8: (a) First cycle of galvanostatic charge-discharge curves at a rate of C/10. (b) Cyclic voltammetry curves for the first cycle at a rate of 0.05 $mV.s^{-1}$. (+) Graphite and (▲) CX-A16.

The first observation is that the charge capacity of the activated carbon xerogel is much higher than that of graphite (Fig. 8a). However, in the case of graphite, the de-insertion of all the Li^+ ions occurs in a narrow potential window (between 0.1 and 0.2 V *vs.* Li^+/Li). This means that the complete capacity is restored at a nearly constant potential value. Increasing the de-insertion potential to a higher value would in this case not provide any additional capacity, as evidenced from the vertical charge curve at potential higher than 0.2 V *vs.* Li^+/Li. On the opposite, in the case of CX, the charge process (de-insertion of Li^+ ions) occurs continuously over the whole potential window (between 0 to 3.0 V *vs.* Li^+/Li), which is reflected by the continuous charge increase versus potential. Due to this continuous increase, carbon xerogels are not suitable for batteries delivering constant power (*i.e.* constant voltage) for the application. Moreover, as mentioned earlier, a capacity at too a high potential value is less useful in a real battery. Indeed, common cathode materials for Li-ion batteries usually display insertion/de-insertion potentials around 3.5 to 4 V *vs.* Li^+/Li. Consequently, the voltage of a full cell would strongly decrease if the potential for the de-insertion from the carbon electrode occurs at too a high value.

Further evidence is given by the comparison of the cyclic voltammetry curves (Fig. 8b). The first main difference between the two materials during the first discharge is mainly attributed to the degradation of the electrolyte at the surface of the CX material, leading to a huge SEI at a potential close to 0.65 V *vs.* Li^+/Li on the cathodic part of the cyclic voltammetry curve (Fig. 8b). This peak is almost undiscernible in the case of graphite. The insertion peak is found to occur at similar potential values (between 0.005 and 0.15 V *vs.* Li^+/Li) in both cases. On the opposite, the de-insertion occurs in a narrow potential range in the case of graphite (reflected by the narrow peak around ~0.23 V *vs.* Li^+/Li), whereas at least three ill-defined peaks can be observed at higher potential values in the case of CX (around 1.2 V, 2.3 V and 3.0 V *vs.* Li^+/Li) indicating a continuous de-insertion over the full range of potential (Fig. 8b). Therefore, the

major difference between these two materials results from a contribution to capacity above 1.5 V *vs.* Li^+/Li, both curves leading to similar capacity values when cycling is performed at this potential. The very different behavior at high potential in terms of Li^+ insertion and de-insertion results from the presence of a large amount of micropores, dominating the specific surface area of the activated carbon in the electrode.

3.5. Effect of the microporosity on electrochemical behavior

Fig. 9a shows the reversible charge capacity at the first charge-discharge cycle as a function of the total accessible specific surface area ($S_{mic,NLDFT}$ + S_W**)** of the CX powders for both series of measurements, *i.e.* using either 1.5 V or 3.0 V *vs.* Li^+/Li as maximum voltage. On the one hand, the reversible charge capacity is almost constant when the potential is limited to 1.5 V *vs.* Li^+/Li, suggesting no direct influence of the micropores. On the other hand, when the charge is carried out up to 3.0 V *vs.* Li^+/Li, the reversible charge capacity increases with the total surface area, for activated carbon xerogels. A direct relationship between S_{tot} and Q_{rev} is found only if two conditions are fulfilled simultaneously: (i) the potential window is increased up to 3.0 V *vs.* Li^+/Li and (ii) the binder used preserves the micropore texture of the pristine materials. Indeed, the absolute values of capacity obtained in the present study are much higher than those found in literature with similar materials. In the case of a physically activated CX, Liu *et al.* [12] report a reversible capacity value of 645 $mAh.g^{-1}$ at a maximal potential of 3.0 V *vs.* Li^+/Li for a specific surface area, S_{BET}, of 2912 $m^2.g^{-1}$. The electrode was however prepared using an organic ink (with PVDF in NMP), which certainly led to a sharp decrease of the microporosity in the resulting active material-binder composite. In the present work, a reversible capacity value of 1330 $mAh.g^{-1}$ is obtained for a lower specific surface area, *i.e.* S_{BET} equal to 2234 $m^2.g^{-1}$. This very high difference can be explained by the aqueous preparation process of the electrodes. Indeed, the method used in the present study (xanthan gum as binder in water) allows for the preservation of the microporous texture of the pristine powder material in the

final composite (Fig. 2). Consequently, it is likely that the micropore fraction really accessible to the electrolyte is much higher than in the work of Liu *et al.* [12].

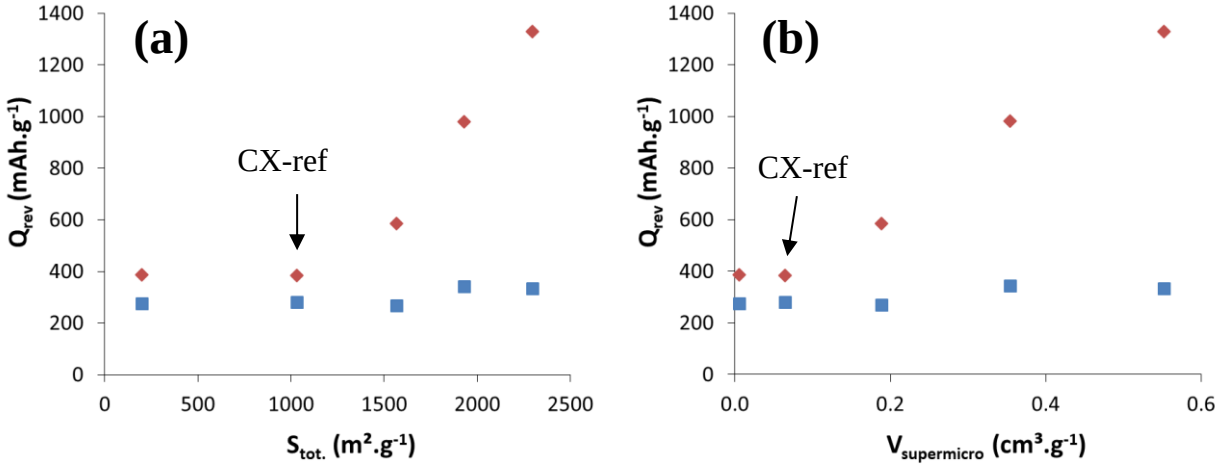

Fig. 9: Reversible capacity at the first charge-discharge cycle (a) as a function of total accessible specific surface area ($S_{mic,NLDFT}$ + S_W) and (b) as a function of the cumulative volume of supermicropores (0.7 – 2 nm). The charge was carried out at a maximum potential of: (■) 1.5 V *vs.* Li^+/Li and (◆) 3.0 *vs.* Li^+/Li.

Considering Fig. 9b, it becomes even more evident that the supermicropore fraction of the material plays a key role in the insertion and de-insertion mechanisms of Li^+ ions. Indeed, a linear increase in reversible capacity is evidenced in this case with the increase in the supermicropore volume of the material, if the charge is carried out up to 3.0 V *vs.* Li^+/Li. In that way, the massive insertion of Li^+ ions at the first discharge is mainly controlled by the large micropores, and their extraction from these pores can only occur at the higher potential values.

Fig. 9 also shows that decreasing the specific surface area using CVD to reduce the accessible micropore volume does not decrease the reversible capacity compared to CX-Ref: Q_{rev} is almost constant, whatever the maximum voltage value. This indicates that, in the case of CX-Ref, the micropores play no role in insertion-deinsertion of Li^+ ions, even when a water-based process is used to prepare the electrode. In this way, in the case of CX-Ref, only the external

surface of the nodules is accessible to the Li^+ ions: micropores are present in the nodules but are not accessible to the electrolyte. As a consequence, the electrode capacity is identical, whatever the maximum charge potential value considered. Physical activation using CO_2 increases the total and in particular the accessible micropore volume and also leads to an enlargement of their size. Such formation of a substantial volume of large micropores (supermicropores: 0.7 to 2 nm) allows for an increased ion accessibility to the structure, and so, a higher Li^+ insertion. Consequently, when activated CX are used as negative electrode (with xanthan gum as a binder), the enlargement of the micropores allows for an access to the electrolyte, and so, the Li^+ ions, leading to increased capacities directly related to the total accessible surface area. Note again that the use of PVDF as a binder would not lead to the same conclusions considering the fact that the microporosity of the porous carbon powder is blocked by PVDF.

4. Conclusions

The modulation of the micropore volume of a carbon xerogel, as quantified by nitrogen and CO_2 adsorption-desorption analysis, was successfully achieved by the use of both CVD with ethylene and CO_2 physical activation. Materials with total surface areas between 200 and 2300 $m^2.g^{-1}$ and nearly constant macropore size and volume, were produced. Li-ion battery electrodes were prepared *via* an original aqueous process using xanthan gum as a binder and water as a solvent. This process allows to preserve the textural characteristics (in particular the accessibility of the micropores) of the CX powders in the final active material-binder composite, which is not the case when PVDF in NMP is used, as in most studies.

Capacitance measurements show a significant improvement of the accessibility of the materials by the electrolyte when activated CX are used. The influence of activation and carbon deposition treatments on the electrochemical behavior of the samples in half-cell was highlighted. Regarding Li^+ insertion during the first cycle, a clear linear dependency could be

evidenced with the increase of the volume of supermicropores (0.7 – 2 nm), demonstrating the effect of micropore enlargement by activation on the storage capacity. While the reversible de-insertion capacity remained constant when the maximum potential value was set at 1.5 V *vs.* Li^+/Li, a clear linear relationship was observed between the supermicropore volume and the reversible capacity at a maximum potential value of 3.0 V *vs.* Li^+/Li. These results indicate that the contribution of the larger micropores of CX materials to the observed Li^+ storage capacity is significant when cycling is performed in a wider potential window and when a water-compatible binder is used for the electrode preparation. Indeed, during the first discharge, Li^+ ions penetrate massively inside the CX micropore structure, but are only partially extracted when the charge of the half-cell is performed up to 1.5 V *vs.* Li^+/Li. The increase of the potential value up to 3.0 V *vs.* Li^+/Li allows for a more pronounced de-insertion of the Li^+ ions from the microporosity of the activated CX.

The present work has provided new information on the behavior of porous carbons when used as anodes for Li-ion batteries. In particular, it has been demonstrated that, to determine the influence of the micropore texture on parameters such as charge or discharge capacity, the pore texture of the active material-binder composite needs to be taken into account: that of the pristine powder could very well be irrelevant. Furthermore, the electrochemical characterization conditions, and especially the potential window used, have to be clearly defined to avoid any wrong conclusions. Indeed, if the potential is increased up to 3.0 V *vs.* Li^+/Li, a larger amount on Li^+ ions can be de-inserted in the case of porous carbons, leading to enhanced (and sometimes quite striking) capacity values; however, charge-discharge up to 3.0 V *vs.* Li^+/Li for a negative electrode is not realistic for practical applications.

Acknowledgements

M.-L. Piedboeuf thanks the F.R.S.-FNRS for a FRIA fellowship grant. A. Léonard and N. Job thank the financial support from the Région Wallonne (BATWAL, grant agreement 1318146, PE Plan Marshall 2.vert) and the Research Funds for Coal and Steel - RFCS (PROMOTEE, grant agreement 709741). The authors also thank the University of Liège (Fonds Spéciaux pour la Recherche FSR C13/09) and the Fonds de Bay for their financial support.

References

[1] T. Nagaura, K. Tozaawa, Lithium Ion rechargeable battery, Prog. Batter. Sol. Cells. 9 (1990) 209–212.

[2] E. Buiel, J.R. Dahn, Li-insertion in hard carbon anode materials for Li-ion batteries, Electrochim. Acta. 45 (1999) 121–130. doi:http://dx.doi.org/10.1016/S0013-4686(99)00198-X.

[3] H. Fujimoto, K. Tokumitsu, A. Mabuchi, N. Chinnasamy, T. Kasuh, The anode performance of the hard carbon for the lithium ion battery derived from the oxygen-containing aromatic precursors, J. Power Sources. 195 (2010) 7452–7456. doi:10.1016/j.jpowsour.2010.05.041.

[4] J. Ni, Y. Huang, L. Gao, A high-performance hard carbon for Li-ion batteries and supercapacitors application, J. Power Sources. 223 (2013) 306–311. doi:http://dx.doi.org/10.1016/j.jpowsour.2012.09.047.

[5] M.-L.C. Piedboeuf, A.F. Léonard, F.L. Deschamps, N. Job, Carbon xerogels as model materials: toward a relationship between pore texture and electrochemical behavior as anodes for lithium-ion batteries, J. Mater. Sci. 51 (2016) 4358–4370. doi:10.1007/s10853-016-9748-3.

[6] N. Job, R. Pirard, J. Marien, J.-P. Pirard, Porous carbon xerogels with texture tailored by pH control during sol–gel process, Carbon N. Y. 42 (2004) 619–628. doi:http://dx.doi.org/10.1016/j.carbon.2003.12.072.

[7] N. Rey-Raap, M.-L.C. Piedboeuf, A. Arenillas, J.A. Menéndez, A.F. Léonard, N. Job, Aqueous and organic inks of carbon xerogels as models for studying the role of porosity in lithium-ion battery electrodes, Mater. Des. 109 (2016) 282–288. doi:10.1016/j.matdes.2016.07.007.

[8] M.S. Contreras, C.A. Páez, L. Zubizarreta, A. Léonard, S. Blacher, C.G. Olivera-Fuentes, et al., A comparison of physical activation of carbon xerogels with carbon dioxide with chemical activation using hydroxides, Carbon N. Y. 48 (2010) 3157–3168. doi:10.1016/j.carbon.2010.04.054.

[9] Z. Yang, Y. Xia, X. Sun, R. Mokaya, Preparation and hydrogen storage properties of zeolite-templated carbon materials nanocast via chemical vapor deposition: Effect of the zeolite template and nitrogen doping, J. Phys. Chem. B. 110 (2006) 18424–18431. doi:10.1021/jp0639849.

[10] Y. Zhu, X. Xiang, E. Liu, Y. Wu, H. Xie, Z. Wu, et al., An activated microporous carbon prepared from phenol-melamine-formaldehyde resin for lithium ion battery anode, Mater. Res. Bull. 47 (2012) 2045–2050. doi:http://dx.doi.org/10.1016/j.materresbull.2012.04.003.

[11] S.J. L. Nian-Ping G. Da-Yong, L. Dong, Z. Xiao-Wei, L. Ya-Jie, Effect of carbon aerogel activation on electrode lithium insertion performance, Acta Physico-Chemica Sin. 29 (2013) 966–972. doi:10.3866/PKU.WHXB201302281.

[12] X. Liu, S. Li, J. Mei, W.-M. Lau, R. Mi, Y. Li, et al., From melamine-resorcinol-formaldehyde to nitrogen-doped carbon xerogels with micro- and meso-pores for lithium batteries, J. Mater. Chem. A. 2 (2014) 14429–14438. doi:10.1039/C4TA02928C.

[13] M.-L.C. Piedboeuf, A.F. Léonard, K. Traina, N. Job, Influence of the textural parameters of resorcinol–formaldehyde dry polymers and carbon xerogels on particle sizes upon mechanical milling, Colloids Surfaces A Physicochem. Eng. Asp. 471 (2015) 124–132. doi:http://dx.doi.org/10.1016/j.colsurfa.2015.02.014.

[14] M. Thommes, K. Kaneko, A.V. Neimark, J.P. Olivier, F. Rodriguez-Reinoso, J. Rouquerol, K.S.W. Sing, Physisorption of gases, with special reference to the evaluation of surface area and pore size distribution (IUPAC Technical Report), Pure Appl. Chem. 87 (2015) 1051–1069.
doi: http://dx.doi.org/10.1515/pac-2014-1117

[15] R.W. Magee, Evaluation of the External Surface Area of Carbon Black by Nitrogen Adsorption, Rubber Chemistry and Technology, 68 (1995) 590-600.
doi:http://doi.org/10.5254/1.3538760.

[16] P. Tarazona, A density functional theory of melting, Mol Phys, 52 (1984) 81-96.
doi: http://doi.org/10.1080/00268978400101071.

[17] P. Tarazona, Free-energy density functional for hard spheres, Phys. Rev. A, 31 (1985) 2672-2679.
doi: http://doi.org/10.1103/PhysRevA.31.2672.

[18] P. Tarazona, M.B. Marconi, R. Evans, Phase equilibria of fluids interfaces and confined fluids: Non-local versus local density functionals, Mol Phys, 60 (1987) 573-595.
doi: http://doi.org/10.1080/00268978700100381

[19] J.P. Olivier, Modeling physical adsorption on porous and nonporous solids using density functional theory, J. Porous Mat., 2 (1995) 9-17.
doi: http://doi.org/10.1007/BF00486565.

[20] M.W. Maddox, J.P. Olivier, K.E. Gubbins, Characterization of MCM-41 using molecular simulation: Heterogeneity effects, Langmuir, 13 (1997) 1737-1745.
doi: https://pubs.acs.org/doi/abs/10.1021/la961068o.

[21] C. Balzer, R.T. Cimino, G.Y. Gor, A.V. Neimark, G. Reichenauer, Deformation of microporous carbons during N_2, Ar, and CO_2 adsorption: Insight from the density functional theory, Langmuir, 32 (2016) 8265–8274.
doi: http://pubs.acs.org/doi/10.1021/acs.langmuir.6b02036

[22] E.W. Washburn, Note on a method of determining the distribution of pore sizes in a porous material, Proc. Natl. Acad. Sci. 7 (1921) 115–116.

[23] G.F.M. Antonio, F. Franco, N. Batalha, M.M. Pereira, Coupling CH_4 pyrolysis with CO_2 activation via reverse Boudouard reaction in the presence of O_2 through a multifunctional catalyst Ni-V-Li/Al_2O_3, J. CO_2 Util. 16 (2016) 458–465. doi:10.1016/j.jcou.2016.10.011.